DIPOLAR MAGNETIC FLUX LEAKAGES FOR PIPELINE RECTANGULAR DEFECT CHARACTERIZATION: ANALYTIC APPROACH

L. U. Daura*, A. Dan-Isa, S. A. Babale
Electrical Engineering Department, Bayero University, Kano.
*ludaura.ele@buk.edu.ng; danisa@buk.edu.ng ; sababale.ele@buk.edu.ng

Keywords: –
Analytical model,
Defect quantification,
Ferromagnetism,
Magnetic flux leakages,
and Polynomial function

Article History: –
Received: July 2019.
Reviewed: August 2019.
Accepted: August 2019.
Published: September.2019.

ABSTRACT

Magnetic Flux Leakages (MFL) find its application in non-invasive of Non-Destructive Testing and Evaluation (NDT&E) to detect and characterized defect in pipelines made from ferromagnetic materials. Various improvements of MFL models have been investigated for defect quantification but still could not achieve higher precision due to technical errors. We, therefore, propose models that minimize the error generated by inverse MFL model for defect quantification. Depth and width polynomial expressions were generated from the peak values of the two MFL profile using polyfit function for their errors' evaluation by varying depth at constant width and varying width at a constant depth. The model gives a prediction of a rectangular defect quantification based on dipolar magnetic charge model from the nature of the axial and radial flux leakages profile. The proposed model used analytic expressions to characterize the defect from the MFL signal. Among the three axes of the MFL profile, only radial and axial profiles were used in this paper to quantify the defect. The model improved the error margin and proved that the radial MFL profile is best for the estimation of defect length along the scan axis direction with nearly zero percent error while the axial MFL profile provides best results for the evaluation of width and depth with 2.20% and 2.18%as maximum percentage error. The proposed Radial and axial leakage profile analytical models are simple and can be used for reconstruction of defect in inverse MFL problem.

1. INTRODUCTION

Our society relies on and requires an extensive pipeline network to transfer and deliver water, gas, oil, etc. from one area to another. In many cases, the pipeline extends over hundreds of miles and run through an inhospitable environment. The pipeline may develop a defect during the production phase and in-service operations. Besides factory and in-service defect, pipes are often subject to natural deformation over time due to the impact of environmental factors like soil, water, climate, natural vegetation, and landforms, etc. Pipeline defects not only would waste resources, but also can be harmful and hazardous to its surrounding terrestrial or aquatic life. The consequences of all these pipeline failures are what brought the idea of pipeline integrity management [1].

Among the different phases of pipeline integrity management, this research paper is based on defect detection and characterization. The detection and characterization of defect can be achieved through pipeline inspection, monitoring, testing, and different techniques for data analysis. Non-Destructive Testing and Evaluation (NDT&E) techniques are used in this research because of its advantages as defined by American society non-destructive testing [2]. There are different NDT&E for defect Quantitative in oil and gas pipeline inspection. The techniques are either applied for In-Line (ILI) Inspection [1], [3] or external inspection method [4]. Magnetic Flux Leakages (MFL) Testing, Eddy Current Testing (ECT), Ultrasonic Testing (UT), Thermography Testing (TT), etc. [1], [3], [5] - [6] are some of the prominent techniques. MFL testing is one of the oldest techniques, evolved in the pipeline inspection

industry before the 1960s and are more widely used in NDT&E techniques [1], [7] - 14]. Its relatively safe, cheap, fast and reliable, non-invasive nature and ability to detect both inner and outer defects when compared to other techniques [13]. Due to the advancement in the sensor technology and signal processing equipment, the MFL technique has been modified to pulse MFL, Direct Current (DC) MFL and Alternating Current (AC) MFL [13], [15] for more efficient/robust to defect characterization. However, the MFL applications on defect characterization are limited to some alloys and ferromagnetic materials up to date [9].

Magnetic flux is directly proportional to the number of magnetic flux lines passing perpendicularly through given specimens. When a magnetic field interacts with a ferromagnetic material, much of that field is enclosed by that material. In the case of a magnetic field generator such as a permanent magnet within a steel pipe, the pipe will restrict the magnetic flux from escaping the pipe. If, however, there is a breach as a result of flaw or corrosion in the pipe wall, the magnetic flux would escape or "leak-out" from the pipeline as shown in Fig. 1(b) [11]. That is what the Magnetic flux leakages testing utilizes in characterizing the flaw in a pipeline. Exclusively, the MFL testing is to detect anomalies in the normal flux pattern created by a discontinuity in a ferrous material when induces by an external field. The source of the induced field is either from traditional permanent magnets [16] or electromagnet [17], [18] or both. Each depends on the direction of the induced field and the type of excitation.

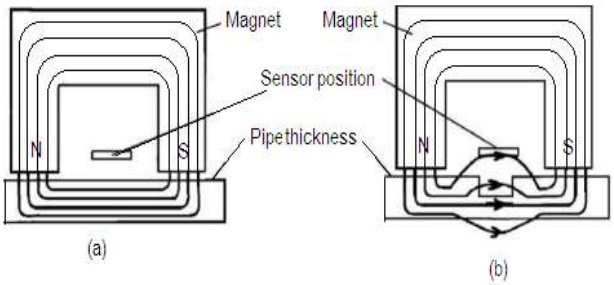

Fig. **1.** Principle of magnetic flux leakage detection. (a) Pipe without defect (b) Pipe with defect.

All known pipeline materials respond with magnetic fields in different ways. The most pronounced response is observed with ferromagnetic materials and more commonly, ferromagnetic metals [19]. Ferromagnetism has multiple uses throughout the industry. One of the more common application is the measurement of many physical quantities such as velocity, displacement, position, acceleration, angular momentum, potential difference, and current indirectly through the analysis of magnetic flux. Many sensors were developed that cater to the measurement of magnetic flux [6], [15], [20] – [21]. This research explores the defect detection based on NDTE&E.

For the model MFL techniques, there are two ground-breaking mathematical approaches which are all based on the solution of Maxwell's equations. Firstly, the magnetic dipole method which was pioneered by Zatsepin and Shcherbinin [22], [23] and secondly, the finite element method which was pioneered by Hwang and Lord [24]. The earliest studied dipole simulations presented the variation of MFL magnitude with defect parameters on the assumption that the induced magnetic charge density is independent of defect parameters. Furthermore, there are qualitative theories to calculate and explain the formation of a uniform magnetic field inside the defect and proved that it depends on the applied field, ferromagnetic permeability, and defect parameters [24] – [27]. Different researches were also conducted on numerical simulation [28], [29]. However, they lack a direct relationship for some defect parameters.

Various qualitative theories explained the formation of the uniform magnetic field inside the defect and showed it depends on the applied field, material permeability and defect parameters as presented for a 2D defect with rectangular cross-section [25]. The density of defect-induced magnetic charge was explicitly shown for the first time that it is directly related to the defect surface shape [30]. This open doors to different researches on defects characterization and a lot have been achieved from the relationship between flux leakage signal and defect parameters.

Minkov proposed the first analytical defect sizing-error quantification based on right angular parallelepiped surface crack. The depth computation gave 2% error for the known crack length and width but when the crack width and length are unknown; the depth error is within 12% while the width error for separate measurement is at most 30% [31]. Minkov

further improved from the insufficient precision error of 21% and 31% for depth and width to 12% and 20% respectively [32]. Based on tangential components, it has been observed that the depth error for crack with higher depth could yield an estimated value below 28% [4]. In another development, Yong proposed particle swamp optimization algorithm on MFL radial profile to observe the error margin for three different cracks in which He obtained a maximum error for two separate trials as 6.67% and 7.37% for crack width and depth respectively [33]. Later, Suresh proposed another error quantification based on analytical cylindrical defect model using only the radial flux leakage profile to 33% for diameter estimation [26]. Another analytical model presented for a rectangular defect shape that quantifies the defect parameters with minimised error for radial (best) MFL profile compared to axial MFL as 2.89% and 0% for depth and length respectively [27]. There are also other proposed analytical models that described how MFL signal related to geometrical shapes of the defect and presented the capabilities of each MFL profile on defect estimation [34] – [37]. It has been observed from the above-reviewed literature that almost all the work on dipole modeling of MFL geared towards using spatial MFL profiles to characterise defect and only the length is directly obtained from the plot of the radial profile.

Of recent, some research was presented using Fourier methods to characterise defect depth directly from the nature of the Fourier plots, which is a development from the previous work [38]. The spatial spectrum of the Fourier method lacks an explanation for a defect with large and minimal width because of non-uniformity of magnetic dipole density in the wall of the slot and the error of MFL testing become larger respectively [38]. In another development, the radial charge density is higher at the defect tip compared to the defect mouth, as shown in dipole modeling of rectangular elements of the crack wall and their superposition [32]. Furthermore, Mandache assumed a constant magnetic charge density for analytical and experimental models that showed the interaction of racetrack defect length estimation based on the locations of the peak radial MFL. However, it could not account for the defect depth [39]. Mandache used the saturation level of the magnetic field and a few parameters to make the knowledge of material characteristics like permeability and coercivity, etc. not necessary. Based on an analytical model, it has been investigated that MFL tangential profile is the best for assessing defect orientation angle compared to the axial profile while the radial profile is prone to substantial error [40]. Therefore, it is an indication that more researches need to carry out to reduce defect quantification error margin for the current state of the art in MFL techniques.

Based on the various stated challenges for error in defect quantifications, we propose radial and axial leakage profile models which are simple and can be used for reconstruction of defect in inverse MFL problem. The remaining parts of the paper are divided into a different section. Section 2 described the methods for achieving the proposed models. Section 3 described the results and discussions from the proposed models, while section 4 is the conclusion and future work.

2. PROPOSED MODEL

This paper, as it's based on defect detection and characterization, it focuses on error minimization for crack quantification using MFL techniques. Three models were developed. The first two models were based on dipolar magnetic charge approach. The third model was from the best curve fitting between the first two models for crack parameters. A MATLAB numerical simulation software was used for the three model's evaluation. The proposed models predict the defect characteristics from the nature of defect parameters. The defect in this paper is considered to be a crack with different length, width, and depth. The cracks are modelled as an artificial slot in a ferromagnetic material. Fig. 2 shows the cuboids defect shape with the length, '*l*' width, '*w*' and depth, 'd'. The scan direction is along the y-axis and assumed *h*=lift off position for the field sensing in the proposed model. Magnetic flux density for a differential element *dB* at a sensor position $p(x,y,h)$ distances R_+ and R_- due to north and south dipoles respectively, and the total flux leakages density is given by equation (1) for x-, y- and z-axis direction.

$$dB = idB_x + jdB_y + kdB_z \quad (1)$$

The differential flux density at any point from a differential pole is given by (2) [5].

$$dB = \frac{\mu m}{4\pi R^2}\vec{r}ds \quad (2)$$

From (2) at a lift-off point p*(x,y,h)*, the flux density, *B*, is given as

$$B = \frac{m}{4\pi}\int \frac{\vec{r}}{R^2}.ds \quad (3)$$

Where,

dB_x is the tangential differential flux density,

dB_y is the axial differential flux density,

dB_z is the radial differential flux density at point p.

Where m = poler charge density in Wb/m^2, and $\vec{r}$ is a unit vector in the direction of R.

ds is the differential area for a dipole region,

The normalized distance from a pole to the field sensing position along z- axis is also given in (4),

$$\vec{r} = \frac{h-z}{R} \quad (4)$$

The distances of the sensor from the dipole North and South Pole positions are given by (5) and (6) as:

$$R_+ = \sqrt{x^2 + y^2 + (h-z)^2} \quad (5)$$

$$R_- = \sqrt{x^2 + (y-l)^2 + (h-z)^2} \quad (6)$$

And the Cartesian differential area is the product differential z- and y- length given as:

$$ds = dzdx \quad (7)$$

or easier formatting of the manuscript and conformity with ZJEET specification requirement, it is recommended that this document as template is strictly complied.

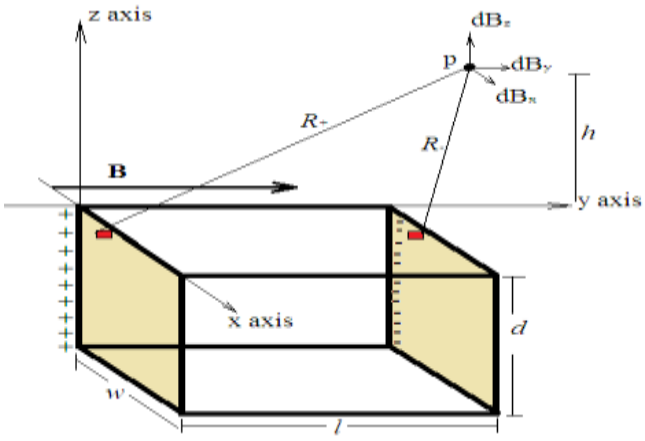

Fig. 2. Cuboid hole defect

2.1 Radial field density

The radial field density is the equivalent field density along the radial axis at a sensing point. Its value is the total contribution of north and south dipole charge density at a lift-off position. This model is obtained by substituting (6) to (9) in (3). Therefore, we have the north and south poles differential field response at the sensing position given by (8) and (9).

$$B_z^+ = \frac{m}{4\pi}\int_0^w \int_{-d}^0 \frac{(h-z)}{(x^2+y^2+(h-z)^2)^{\frac{3}{2}}} dzdx \quad (8)$$

$$B_z^- = \frac{-m}{4\pi}\int_0^w \int_{-d}^0 \frac{(h-z)}{(x^2+(y-l)^2+(h-z)^2)^{3/2}} dzdx \quad (9)$$

Finally; the contribution of north and south dipole in (8) and (9) were evaluated and presented in (10) and (11) each as a function of crack width, length and depth for a given sensing position, lift-off (h).

$$B_z^+ = \frac{m}{4\pi}\ln\left(\frac{\left(\frac{\sqrt{w^2+y^2+h^2}+w}{\sqrt{w^2+y^2+(h+d)^2}+w}\right)}{\left(\sqrt{[y^2+h^2]/[y^2+(h+d)^2]}\right)}\right) \quad (10)$$

$$B_z^- = \frac{-m}{4\pi}\ln\left(\frac{\left(\frac{\sqrt{w^2+(y-l)^2+h^2}+w}{\sqrt{w^2+(y-l)^2+(h+d)^2}+w}\right)}{\left(\sqrt{[(y-l)^2+h^2]/[(y-l)^2+(h+d)^2]}\right)}\right) \quad (11)$$

The equivalent radial field density is the total contribution of the north and south dipole given in (10) and (11). Therefore,

$$B_z = B_z^+ + B_z^- \quad (12)$$

2.2 Axial field density

The axial field density is the equivalent field density along the axial direction at a sensing point. Its value is the total contribution of north and south dipole charge density at a lift-off position. Similarly, the model is obtained by substituting (6) to (9) in (3). Therefore, we have the north and south poles differential field response at the sensing position given by (13) and (14).

$$B_y^+ = \frac{m}{4\pi}\int_0^w \int_{-d}^0 \frac{y}{(x^2+y^2+(h-z)^2)^{\frac{3}{2}}} dzdx \quad (13)$$

$$B_y^- = \frac{-m}{4\pi}\int_0^w \int_{-d}^0 \frac{y}{(x^2+(y-l)^2+(h-z)^2)^{3/2}} dzdx \quad (14)$$

Finally; the contribution of north and south dipole in (13) and (14) were evaluated and presented in (15) and (16) each as a function of crack width, length and depth for a given sensing position, lift-off (h).

$$B_y^+ = \frac{m}{4\pi}\left[-\tan^{-1}\left(\frac{y\coth\left(\sinh^{-1}\frac{w}{\sqrt{y^2+(h+d)^2}}\right)}{(h+d)}\right) + \tan^{-1}\left(\frac{y\coth\left(\sinh^{-1}\frac{w}{\sqrt{y^2+h^2}}\right)}{h}\right)\right] \quad (15)$$

$$B_y^- = \frac{-m}{4\pi}\left[-\tan^{-1}\left(\frac{(y-l)\coth\left(\sinh^{-1}\frac{w}{\sqrt{(y-l)^2+(h+d)^2}}\right)}{(h+d)}\right) + \tan^{-1}\left(\frac{(y-l)\coth\left(\sinh^{-1}\frac{w}{\sqrt{(y-l)^2+h^2}}\right)}{h}\right)\right] \quad (16)$$

The equivalent axial field density is the total contribution of the north and south dipole given in (15) and (16). Therefore,

$$B_y = B_y^+ + B_y^- \quad (17)$$

The derived models from radial and axial profile of flux density are evaluated for error minimisation on MFL testing. The models are the true reflection of actual cracks models that can be used for reconstruction during inverse problems.

2.3 Polynomial fit model

We derived the polynomial models for width and depth from the data of the axial and radial models described in section 3 above. A MATLAB numerical simulation software was used to evaluate the developed polynomial functions of depth and width. The models find the coefficients of a polynomial with the best degree that fits the data in a least-squares sense to obtain error estimates for predictions in a set of data. For the defect depth error estimation, we derived two depth-polynomials from the axial and radial profile as a function of maximum MFL signals for varying depth from 2mm to 7mm at a constant width. Whereas, for the case of width error, we also derived another two width-polynomials from the axial and radial profile as a function of maximum MFL signals using various width from 2mm to 7mm at a constant depth. The selected values, 2mm to 7mm are within the range of standard physical pipeline thickness.

3. RESULTS AND DISCUSSION

Crack based on cuboidal defect as in Fig. 2 is modelled in (12) and (17). The developed models depend on cracks parameters. The error of each model is evaluated by taking one parameter as the model variable and keep the remaining as constant. The considered parameters are the crack width and depth for a constant lift-off and crack length. Various results were evaluated in MATLAB software based on crack depth and width. Depth and width polynomial models were also developed to compute the error margins and compare with the previous work in the field.

Fig. 3 shows the radial and axial field leakage profile obtained from the model for a rectangular defect with the length of 6mm, a width of 1.5 mm and various depth. Fig. 3 (a) shows that there are two peak points' features; one is positive while the other is negative. The two points are the point immediately before and after the crack, where the flux density is higher. Their width depends on the crack width. Besides, the higher the defect depth, the higher the peak value of the two points. Therefore, the values of the field density and the scan point at the two peak points have information related to the crack width and depth. Fig. 3(b) shows the axial leakage profile obtained from the axial model under the same condition with the radial model.

Similarly, it shows that the higher the peak value, the higher the crack depth. But as the depth decreases to 1.5 mm, the peak value splits into two. There is also zero crossing points for each crack signal. The points at which it crosses zero depends on the width of the crack.

Similarly, Fig. 4 shows the radial and axial field leakage profile obtained from the model for a rectangular defect with the length of 6mm, depth of 1.5 mm, and various width. Fig. 4 (a) shows that there are two peak points' features; one is positive while the other is negative. The two points show the same position as that of various depth in Fig. 3(a).

Furthermore, Fig. 4(b) follows the same pattern with that of Fig. 3(b) above. These show that the depth and width of the crack have an impact on the crack models. Based on the peak values of the two models for various depth and width, the model is more sensitive to crack depth than width.

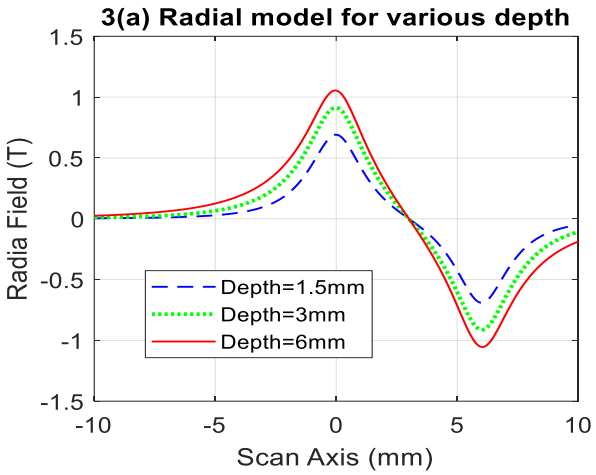

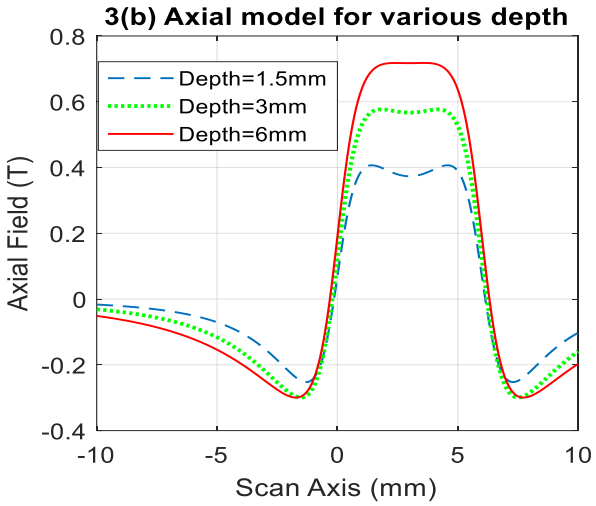

Fig. 3. Radial and Axial Magnetic Flux Leakage Density for 1.5 mm width

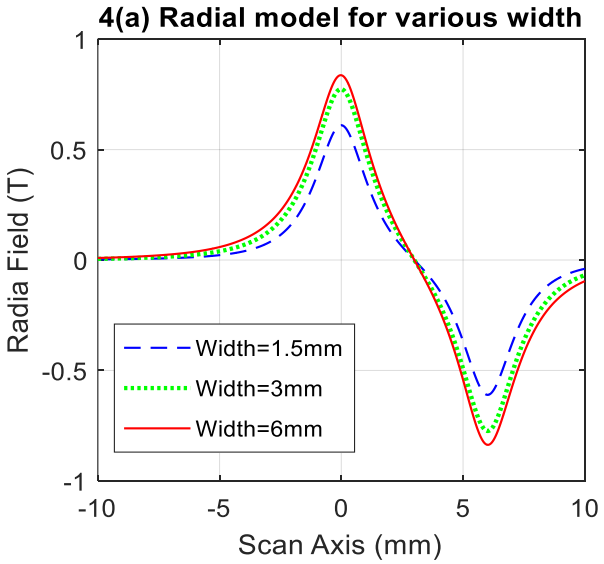

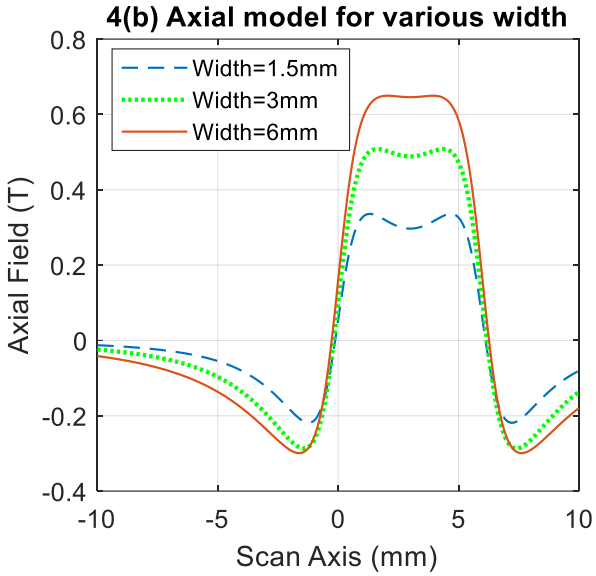

Fig. 4. Radial and Axial Magnetic Flux Leakage Density for 1.5 mm depth

The length of the crack is directly obtained from the features extracted in Fig. 4 (a) and (b). The features are the two peak values in Fig. 3(a) and 4(a) two crossing points in Fig. 3(b) and 4(b). The distance between peak to peak presented by Fig. 3(a) and 4(a) show almost 0% error for crack length measurement. Whereas, the distance of the two zero crossing point in Fig. 3(b) and 4(b) show the crack length with approximately 10% error for 6 mm length. Therefore, the radial model gives the best crack length estimation compared to the axial model. The crack width and depth have no direct relationship with the features of the two models. In the next paragraph, the crack depth and width impact have been evaluated for obtaining the exact error of the two models' crack quantification.

From the two models, it is observed that for constant width, the depth of the defect is responsible for peak amplitude of the leakage profile. Similarly, for constant depth, the width is accountable for the peak amplitude of the leakage profile. Therefore, the peak value of the models depends on the crack width and depth.

Polynomial expressions are derived based on the curve which fit between depth and its corresponding amplitude for fixed width and another curve which fit between the width and its corresponding amplitude for fixed depth based on polyfit function of MATLAB Simulink ®. Depth and width are from the maximum

values of radial and axial leakage profile of varying depth at constant width and also for varying width at a constant depth. The axial length is considered to be from -10mm to 10mm in the step of 0.00001, and the variation of width and depth is from 2mm to 7mm in the step of 0.5.

The defect depth and width estimations were evaluated for both the radial and axial models. The polynomial expression for depth and width of the cracks are expressed for both the axial and radial leakage profiles and presented in equation (18).

$$\begin{bmatrix} Depth_{axial} \\ Width_{axial} \\ Depth_{radial} \\ Width_{radial} \end{bmatrix} = \begin{bmatrix} 273.1 & -436.8 & 242.3 & -43.9 \\ 115.8 & -192.2 & 113.7 & -21.1 \\ 1694.7 & -4366.2 & 37518 & -1072.6 \end{bmatrix} \times \begin{bmatrix} \max(b_y)^3 & \max(b_y)^3 & \max(b_z)^3 & \max(b_z)^3 \\ \max(b_y)^2 & \max(b_y)^2 & \max(b_z)^2 & \max(b_z)^2 \\ \max(b_y) & \max(b_y) & \max(b_z) & \max(b_z) \\ 1 & 1 & 1 & 1 \end{bmatrix} \quad (18)$$

Where the peak amplitude of axial leakage profile is represented as B_y and the peak amplitude of the radial leakage profile is represented by B_z.

Table 1 and 2 show the percentage depth and width estimation error for the axial and radial models based on polyfit models. The maximum percentage of error for depth estimation from the axial and radial profiles were found to be 2.17% and 3.77% respectively while that of width estimation errors were 2.20% and 7.11% for the axial and radial profile respectively. From the result, the axial profile has minimum error compared to the radial profile, which is contrary to the model presented by [27, 33, 35].

Table 1 Depth estimation error @ lift off, h=1mm

Actual Depth (@ Width=2mm) (mm)	**Radial Field Estimated Depth (mm)**	**Axial Field Estimated Depth (mm)**	**Radial Field Depth Percentage error (%)**	**Axial Field Depth Percentage Error (%)**
2.00	1.97	1.98	1.37	1.02
2.50	2.59	2.55	-3.77	-2.18
3.00	2.97	3.00	0.89	0.00
3.50	3.41	3.46	2.34	1.14
4.00	3.94	3.96	1.42	1.00
4.50	4.50	4.49	-0.09	0.25
5.00	5.06	5.02	-1.21	-0.46
5.50	5.58	5.54	-1.56	-0.81
6.00	6.07	6.04	-1.12	-0.71
6.50	6.50	6.51	0.01	-0.13
7.00	6.88	6.94	1.69	0.88

Table 2 Width estimation error@ lift off, h=1mm

Actual width (@ Depth=2mm) (mm)	**Radial Field Estimated Width (mm)**	**Axial Field Estimated Width (mm)**	**Radial Field width Percentage Error (%)**	**Axial Field width Percentage Error (%)**
2.00	1.96	1.98	1.78	1.08
2.50	2.68	2.55	-7.13	-2.20
3.00	2.86	3.00	4.69	-0.10
3.50	3.32	3.46	5.13	1.12
4.00	3.95	3.96	1.23	1.04
4.50	4.60	4.49	-2.22	0.32
5.00	5.19	5.02	-3.78	-0.43
5.50	5.69	5.55	-3.47	-0.84
6.00	6.10	6.05	-1.73	-0.76
6.50	6.44	6.51	0.96	-0.16
7.00	6.71	6.93	4.20	0.93

The proposed models' performance has compared with the existing models of MFL techniques. The existing models compared with our presented models, have the crack at the origin of the axes. Therefore, for comparison, the axes of the proposed models presented in Fig. 3. (a) and 4(b) are shifted to have a crack at the origin as it's presented in the existing models [27], [34] – [36]. The comparison is for crack with 6 mm length, 1 mm width and 2.3 mm depth from the proposed and existing models. Fig. 4 shows the models of the four different existing MFL and our proposed one. All the curves follow the same pattern with the proposed model with the exception of the curve by Bin L. presented in [34]. This reason is that the B. Liu model has a scan direction opposite to the proposed model.

In comparison to the error margin for the four existing models, Minkov first model [31] could only improve the error margin for width and depth estimation analytically from 12% and 30% while the second model [32] to 12% and 20%. Later, Amineh model only achieved less than 28% and negligible width impact [4]. Furthermore, a model by Zhang [33] improved to 6.67% and 7.37% less than that of Suresh model [27] that achieved 2.89% as depth error measurement. Our models achieved up to 2.17% as maximum depth error and 2.20% as maximum width error using the modified polyfit function of third order polynomial. This model also proved that axial MFL profile could give the best results compared to radial MFL profile, which is contrary to the previous dipole model.

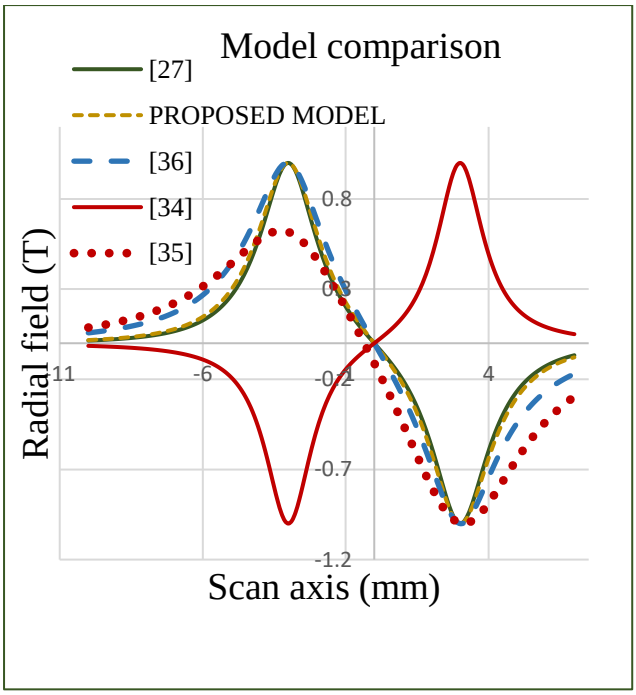

Fig. 4. Comparison of Existing Models

4. CONCLUSION

In this paper, the results of a simple analytical model for Radial and Axial leakage profile of MFL for the rectangular defect is presented. Length, width, and depth of the flaws were estimated from the result of the proposed analytical model. Radial and axial leakage profile have determined the actual defect length with nearly 0% and 10% error respectively for

6mm length, 2mm width, 6mm depth, and 1mm lift-off. The width and depth of the defect are best furnished by the axial magnetic flux leakages with 2.20% and 2.2.18% as maximum errors respectively. All the width and depth errors are obtained based on polyfit Matlab function of degree three. The proposed Radial and axial leakage profile analytical expressions are simple and can be used for reconstruction of defect in inverse MFL problem

Our future work would focus on dipole models on the sample surfaces adjacent to a defect and considering the field-dependent variation of permeability around the defect. This consideration will reduce the error due to the assumption of constant permeability around and inside the defect. Also, an experimental and numerical simulation to validate our models will be studied as part of the future work.

5. ACKNOWLEDGEMENT

The author acknowledges the partial support by the Bayero University, Kano Nigeria under study fellowship and sponsor program.

REFERENCES

[1] Z. T. Mingjiang Xie, "A review on pipeline integrity management utilizing in-line inspection data," *Engineering Failure Analysis,* vol. 92 pp. 222–239, 22 May 2018, 2018.

[2] ASNDT, "Introduction to Nondestructive Testing," American Society For Nondestructive Testing, © Copyright 2017

[3] R. L. Qingshan Feng, Baohua Nie, Shucong Liu, Lianyu Zhao and Hong Zhang, "Literature Review: Theory and Application of In-Line Inspection Technologies for Oil and Gas Pipeline Girth Weld Defection," *Sensors,* vol. 17, no. 50, 2017.

[4] R. K. Amineh, N. K. Nikolova, J. P. Reilly *et al.*, "Characterization of Surface-Breaking Cracks Using One Tangential Component of Magnetic Leakage Field Measurements," *IEEE Transactions on Magnetics,* vol. 44, no. 4, pp. 516-524, 2008.

[5] C. K. W. Okolo, "Modelling and Experimental Investigation of Magnetic Flux Leakage Distribution for Hairline Crack Detection and Characterization," Wolfson Centre for Magnetics, School of Engineering, Cardiff University, unpublish PhD Thesis, 2018.

[6] J. E. Lenz, "A review of magnetic sensors," *Proceedings of the IEEE,* vol. 78, no. 6, pp. 973-989, 1990.

[7] B. C. Liu, Y. Zhang, H. Lin, Y. R. Sun, W. R. Xu, B., "Weak magnetic flux leakage: A possible method for studying pipeline defects located either inside or outside the structures," *NDT & E International,* vol. 74, pp. 81-86, 2015/09/01, 2015.

[8] K. Sakai, K. Morita, Y. Haga *et al.*, "Automatic Scanning System for Back-Side Defect of Steel Structure Using Magnetic Flux Leakage Method," *IEEE Transactions on Magnetics,* vol. 51, no. 11, pp. 1-3, 2015.

[9] Y. Ege, and M. Coramik, "A new measurement system using magnetic flux leakage method in pipeline inspection," *Measurement,* vol. 123, pp. 163-174, 2018/07/01/, 2018.

[10] M. Coramik, and Y. Ege, "Discontinuity inspection in pipelines: A comparison review," *Measurement,* vol. 111, pp. 359-373, 2017/12/01/, 2017.

[11] H. Q. Pham, Q. T. Trinh, D. T. Doan *et al.*, "Importance of Magnetizing Field on Magnetic Flux Leakage Signal of Defects," *IEEE Transactions on Magnetics,* vol. 54, no. 6, pp. 1-6, 2018.

[12] M. R. Kandroodi, B. N. Araabi, M. M. Bassiri *et al.*, "Estimation of Depth and Length of Defects From Magnetic Flux Leakage Measurements: Verification With Simulations, Experiments, and Pigging Data," *IEEE Transactions on Magnetics,* vol. 53, no. 3, pp. 1-10, 2017.

[13] A. T. M. Chukwunonso K. Okolo, "Pulsed magnetic flux leakage method for hairline crack detection and characterization," *American Institute of Physics,* vol. 8, pp. 047207/1 - 047207/12, 2018.

[14] Y. Shi, C. Zhang, R. Li *et al.*, "Theory and Application of Magnetic Flux Leakage Pipeline Detection," *Sensors,* vol. 15, no. 12, 2015.

[15] P. Wang, L. Xiong, Y. Sun *et al.*, "Features extraction of sensor array based PMFL technology for detection of rail cracks," *Measurement,* vol. 47, pp. 613-626, 2014/01/01/, 2014.

[16] H. M. Kim, H. R. Yoo, and G. S. Park, "A New Design of MFL Sensors for Self-Driving NDT Robot to Avoid Getting Stuck in Curved Underground Pipelines," *IEEE Transactions on Magnetics,* 2018.

[17] A. G. Antipov, and A. A. Markov, "3D simulation and experiment on high speed rail MFL inspection," *NDT & E International,* vol. 98, pp. 177-185, 2018/09/01/, 2018.

[18] Y. Feng, L. Zhang, and W. Zheng, "Simulation analysis and experimental study of an alternating current field measurement probe for pipeline inner inspection," *NDT & E International,* vol. 98, pp. 123-129, 2018/09/01/, 2018.

[19] M. P. W. K. H. Panofsky, *Classical Electricity and Magnetism*, Second Edition ed.: Dover Publications Inc, 2005.

[20] H. G. Ramos, and A. L. Ribeiro, "Present and Future Impact of Magnetic Sensors in NDE," *Procedia Engineering,* vol. 86, pp. 406-419, 2014/01/01/, 2014.

[21] Y. He, F. Luo, M. Pan *et al.*, "Defect classification based on rectangular pulsed eddy current sensor in different directions," *Sensors and Actuators A: Physical,* vol. 157, no. 1, pp. 26-31, 2010/01/01/, 2010.

[22] V. E. S. N. N. Zatatsepin, "On calculation of the magnetostatic field of surface defects. Part 1. Topography of the fields of flaw models," *Defektoskopiya*, no. 5, pp. 50-59, 1966.

[23] V. E. P. Shcherbinin, A. I., "On the volume polarization of cracks," *Soviet Journal of Nondestructive Testing,* vol. 10, no. 4, pp. 460-463, May 1975, 1975.

[24] J. H. H. a. W. Lord, "Finite Element Modeling of Magnetic Field/Defect Interactions," *Journa of Testing and Evaluatio,* vol. 3, no. 1, pp. 21-25, 1975.

[25] F. Förster, "New findings in the field of non-destructive magnetic leakage field inspection," *NDT International,* vol. 19, no. 1, pp. 3-14, 1986/02/01/, 1986.

[26] A. A. V. Suresh, "An Analytical Model for Prediction of Magnetic Flux Leakage from Surface Defects in Ferromagnetic Tubes," *MEASUREMENT SCIENCE REVIEW,* vol. 16, no. 1, pp. 8-13, 2016.

[27] V. Suresh, and A. Abudhair, "Dipole Model to Predict the Rectangular Defect on Ferromagnetic Pipe," *Journal of Magnetics,* vol. 21, no. 3, pp. 437-441, 2016.

[28] Y. Li, G. Y. Tian, and S. Ward, "Numerical simulation on magnetic flux leakage evaluation at high speed," *NDT & E International,* vol. 39, no. 5, pp. 367-373, 2006/07/01/, 2006.

[29] G. Zhihua, and C. Xiuli, "Numerical simulation on magnetic flux leakage testing of the steel cable at different speed title." pp. V3-316-V3-319.

[30] S. Lukyanetsa, A. Snarskiib, M. Shamoninc *et al.*, "Calculation of magnetic leakage field from a surface defect in a linear ferromagnetic material: an analytical approach," *NDT & E International,* vol. 36, no. 1, pp. 51-55, 2003/01/01/, 2003.

[31] D. Minkov, J. Lee, and T. Shoji, "Study of crack inversions utilizing dipole model of a crack and Hall element measurements," *Journal of Magnetism and Magnetic Materials,* vol. 217, no. 1, pp. 207-215, 2000/07/01/, 2000.

[32] D. Minkov, Y. Takeda, T. Shoji *et al.*, "Estimating the sizes of surface cracks based on Hall element measurements of the leakage magnetic field and a dipole model of a crack," *Applied Physics A,* vol. 74, no. 2, pp. 169-176, 2002/02/01, 2002.

[33] Y. Zhang, and Z. Ye, "Particle swarm optimisation algorithm for crack shape reconstruction in magnetic flux leakage nondestructive testing," *Nondestructive Testing and Evaluation,* vol. 24, no. 1-2, pp. 243-250, 2009/03/01, 2009.

[34] B. Liu, L.-y. He, H. Zhang *et al.*, "The axial crack testing model for long distance oil-gas pipeline based on magnetic flux leakage internal inspection method," *Measurement,* vol. 103, pp. 275-282, 2017/06/01/, 2017.

[35] G. Kopp, and H. Willems, "Sizing limits of metal loss anomalies using tri-axial MFL measurements: A model study," *NDT & E International,* vol. 55, pp. 75-81, 2013/04/01, 2013.

[36] J. Wu, Y. Sun, Y. Kang *et al.*, "Theoretical Analyses of MFL Signal Affected by Discontinuity Orientation and Sensor-Scanning Direction," *IEEE Transactions on Magnetics,* vol. 51, no. 1, pp. 1-7, 2015.

[37] W. S. Singh, S. V. S. Kumar, C. K. Mukhopadhyay *et al.*, "Modeling and Experimental Studies on 3D-Magnetic Flux Leakage Testing for Enhanced Flaw Detection in Carbon Steel Plates," *Research in Nondestructive Evaluation*, pp. 1-16, 2018.

[38] E. Li, Y. Kang, J. Tang *et al.*, "Analysis on Spatial Spectrum of Magnetic Flux Leakage Using Fourier Transform," *IEEE Transactions on Magnetics*, pp. 1-10, 2018.

[39] L. C. Catalin Mandache, "A model for magnetic flux leakage signal predictions," *Journal of Physics D: Applied Physics,* vol. 36, no. 20, pp. 2427, 2003.

[40] J. S. Alaric, V. Suresh, A. Abudhahir *et al.*, "Theoretical Analysis of the Rectangular Defect Orientation using Magnetic Flux Leakage," *Measurement Science Review,* vol. 18, no. 1, pp. 28-34, 2018.